Nonmagnetic nanocomposites for optical and infrared negative-refractive-index media

Robyn Wangberg and Justin Elser

Department of Physics, Oregon State University, 301 Weniger Hall, Corvallis, Oregon 97331

Evgenii E. Narimanov

Department of Electrical Engineering, Princeton University, Princeton, New Jersey 08540

Viktor A. Podolskiy

Department of Physics, Oregon State University, 301 Weniger Hall, Corvallis, Oregon 97331

Received June 29, 2005; revised August 11, 2005; accepted August 21, 2005

We develop an approach to use nanostructured plasmonic materials as a nonmagnetic negative-refractive-index system at optical and near-infrared frequencies. In contrast to conventional negative-refraction materials, our design does not require periodicity and thus is highly tolerant to fabrication defects. Moreover, since the proposed materials are intrinsically nonmagnetic, their performance is not limited to the proximity of a resonance, so the resulting structure has relatively low loss. We develop the analytical description of the relevant electromagnetic phenomena and justify our analytic results via numerical solutions of Maxwell equations. © 2006 Optical Society of America

OCIS codes: 160.4760, 110.2990, 350.5730.

1. INTRODUCTION

The electromagnetic response of negative refractive index materials (NIM)[1–8] has recently attracted unprecedented attention. Novel optical phenomena predicted to take place in these unique systems include the reversal of Snell's Law, the Doppler effect, the Cherenkov effect,[1] aberration-free[1,2,5] and subdiffraction[3,9–17] imaging, and excitation of the new types of surface and nonlinear waves.[8,18] In particular, realization of NIMs may potentially lead to fabrication of new types of lenses and prisms,[1,3,5] new lithographic techniques,[9,16,17] novel radars, sensors, and telecommunication systems. However, despite the great advantages NIM has to offer for optical and infrared spectral range, all practical realizations of NIM are currently limited to gigahertz frequencies.[19–23]

Until recently there were two major approaches for NIM design. The first one is based on the original proposal[1] that material with simultaneously negative dielectric permittivity and magnetic permeability must have a negative refractive index. This particular approach also benefits from the possibility to resonantly excite the plasmon polariton waves at the interface between NIM and surrounding media, which in turn may lead to subdiffraction imaging.[3,9–13,24] However, the absence of natural magnetism at high (optical or infrared) frequencies[25] requires the design and fabrication of nanostructured metamaterials to achieve nontrivial magnetic permeability.[20,26–31] As these engineered systems typically operate in close proximity to resonance, resonant losses become the dominant factor in system response, severely limiting the practicality of resonant-based systems.[10–13,32]

The second approach for NIM design involves the use of photonic crystals.[4,21–23,34,35] However, the NIM response in these systems is typically associated with second- or other higher-order bands and requires a complete bandgap between the band in use and the next band. The dispersion and very existence of the required bandgap are typically strongly affected by crystal disorder, unavoidable during the fabrication step. The manufacturing of the optical photonic-crystals-based NIM typically requires three-dimensional patterning with accuracy of the order of 10 nm, which is beyond the capabilities of modern technology.

To address the above-mentioned shortcomings of the traditional NIM schemes, we have recently introduced an alternative approach to design NIM structures.[7] In contrast to "conventional" systems, the proposed design does not rely on either magnetism or periodicity to achieve negative refraction response. It has been shown that the combination of strong anisotropy of the dielectric constant and planar waveguide geometry yields the required negative phase velocity in the system.[7] Here we present a detailed description of NIMs proposed in Refs. 7 and 36, study the effects related to waveguide boundaries, important for optical domain, and suggest several nanostructured materials providing the low-loss negative refraction response at optical and infrared frequencies.

The rest of the paper is organized as follows: Section 2 is devoted to electromagnetic (EM) wave propagation in strongly anisotropic waveguides; Section 3 describes the proposed realizations of the structure; imagining properties of these composites are shown in Section 4; and Section 5 concludes the paper.

0740-3224/06/030498-8/$15.00

2. NEGATIVE REFRACTION IN STRONGLY ANISOTROPIC WAVEGUIDES

We consider wave propagation in the two-dimensional planar waveguide structure shown in Fig. 1. The propagation in the system is allowed in the y and z directions, while the waveguide walls occupy the regions $|x|>d/2$. The waveguide core is assumed to be a homogeneous, nonmagnetic ($\mu=1$) material, with a uniaxial anisotropic dielectric constant with dielectric permittivities $\epsilon_\perp$ and $\epsilon_\parallel$ along and perpendicular to the optical axis, respectively. The optical axis of the core material (C) is assumed to be perpendicular to the direction of the wave propagation in the media ($C\|x$). Therefore, despite the anisotropy of the system, the effective refractive index of propagation in the planar geometry waves will be completely isotropic.

Any wave propagating in the system can be represented as a linear combination of the waveguide modes.[7,25] An individual mode is defined by its structure along the optical axis direction (C) and its polarization. Two different kinds of mode have to be distinguished. The modes of the first kind (known as TE waves) have their E vector perpendicular to the optical axis. The propagation of these waves is fully described by the in-plane dielectric constant $\epsilon_\parallel$. The modes of the second kind (known as TM waves) have their H vector in the waveguide plane and are affected by both $\epsilon_\perp$ and $\epsilon_\parallel$. The existence of these TM waves is crucial for the NIM described here.

In the analytical results presented below we limit ourselves to the case of single-mode propagation. We note that such a description provides complete information about the linear properties of the waveguide structure. Indeed, as mentioned above, an arbitrary wave packet in the system can be represented as a linear combination of modes. In our numerical simulations discussed in Section 4, we utilize this property to compute the imaging performance of the system.

A. Waveguide with Perfectly Conducting Walls

As was shown in Ref. 7, the propagation of a mode in a planar waveguide can be described by the free-space-like dispersion relation

$$k_y^2 + k_z^2 = \epsilon\nu\mathrm{k}^2, \tag{1}$$

where ϵ is $\epsilon_\parallel$ for TE modes and $\epsilon_\perp$ for TM ones, k_y and k_z are the propagation components of the wave vector, and $\mathrm{k}=\omega/c$ (with ω and c being the free-space angular frequency of the radiation and the speed of light in a vacuum, respectively). The propagation constant ν is given by

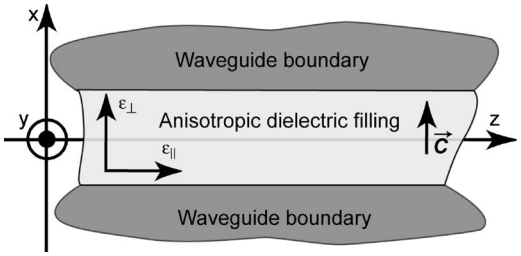

Fig. 1. Schematic configuration of nonmagnetic negative-refraction system.

$$\nu = 1 - \frac{\kappa^2}{\epsilon_\parallel \mathrm{k}^2}, \tag{2}$$

and the parameter κ defines the mode structure in the x direction.[37]

As directly follows from Eq. (1), the phase velocity of a propagating mode is equal to

$$v_p = n\mathrm{k}, \tag{3}$$

where the effective refraction index $n^2=\epsilon\nu$. Note that similar to the case of the plane-wave propagation in free space, the refraction index contains a product of two (mode-specific) scalar constants. A transparent structure must have both propagation constants of the same sign. The case of positive ϵ and ν corresponds to conventional (positive refraction index) material. The case of negative ϵ and ν describes NIM.[7,36] The NIM behavior can be easily illustrated by comparing the Poynting vector S_z and the wavevector k_z, as shown below.

Similar to any waveguide structure, the mode in the system described here can be related to the x profile of the longitudinal field component; a detailed description of such a dependence is given in Ref. 7. To better illustrate the physical picture behind the mode propagation, in this section we present the results for the important case of perfectly conducting waveguide walls. In this case, the EM energy is confined to the waveguide core and the longitudinal field has a $\cos(\kappa x)$ or $\sin(\kappa x)$ profile, depending on the symmetry with respect to the $x=0$ plane, with $\kappa=(2j+1)\pi/d$ for symmetric and $\kappa=2\pi j/d$ for antisymmetric modes, with the integer mode number j. The deviation from this idealized picture due to finite conductance of the waveguide material does not change the physical picture described in this section, and for the practical case of "good" metals (Ag, Al, and Au) at near-IR to terahertz frequencies can be treated perturbatively. The results of such a perturbation approach are presented in Subsection 2.B.

The electric (U_E) and magnetic (U_H) field contributions to the energy density of a mode in weakly dispersive material ($|\epsilon/\omega| \gg |\mathrm{d}\epsilon/\mathrm{d}\omega|$) are given by $U_E=(1/8\pi d)\int(\mathbf{D}\cdot\mathbf{E}^*)\mathrm{d}x$ and $U_H=(1/8\pi d)\int(\mathbf{H}\cdot\mathbf{H}^*)\mathrm{d}x$, respectively[25] (the asterisk denotes the complex conjugation). Using the explicit mode structure for TE and TM waves (see Ref. 7) we arrive at

$$U_E^{(\mathrm{TM})} = U_H^{(\mathrm{TM})} = \frac{1}{16\pi}\frac{\epsilon_\parallel^2\mathrm{k}^2}{\kappa^2}|A_0|^2,$$

$$U^{(\mathrm{TM})} = U_E^{(\mathrm{TM})} + U_H^{(\mathrm{TM})} = \frac{\epsilon_\parallel^2\mathrm{k}^2}{8\pi\kappa^2}|A_0|^2, \tag{4}$$

$$U_E^{(\mathrm{TE})} = U_H^{(\mathrm{TE})} = \frac{\epsilon_\parallel}{16\pi}|A_0|^2,$$

$$U^{(\mathrm{TE})} = U_E^{(\mathrm{TE})} + U_H^{(\mathrm{TE})} = \frac{\epsilon_\parallel}{8\pi}|A_0|^2, \tag{5}$$

where A_0 is the mode amplitude. Thus, extending the similarity between the waveguide system described here

and the free-space propagation, the EM energy of any propagating wave is always positive and contains equal contributions from the electric and magnetic components of the field.

It is also seen that the TE mode is in some sense very similar to the conventional plane wave propagating in the isotropic homogeneous dielectric. Namely, (i) energy density of the TE waves is exactly equal to that of the plane waves and (ii) there is no wave propagation in material with $\epsilon_{\|}<0$. In contrast to this behavior, the sign of the dielectric permittivity alone does not impose limitations on the propagation of TM modes.

Another important characteristic of the energy transport in the EM system is the average energy flux given by the propagating component of the Poynting vector $\mathbf{S}=(c/4\pi)[\mathbf{E}\times\mathbf{H}]$. Selecting the direction of the wave propagation as z axis, we obtain

$$S_z^{(\mathrm{TE,TM})}=c\frac{k_z}{\epsilon_{(\|,\perp)}\mathbf{k}}U^{(\mathrm{TE,TM})}. \tag{6}$$

It is clearly seen from Eq. (6) that the relation between the direction of the phase velocity and direction of the energy flux is defined by the sign of the dielectric constant (for a given mode polarization)—positive ϵ means $n>0$ propagation, whereas $\epsilon<0$ signifies the NIM case. Of course, for this relation to take place, we must require the medium to be transparent; both propagation constants ϵ and ν must be of the same sign. As it can be seen from Eq. (1), the NIM condition can be satisfied only for the TM wave and only in the case of extreme anisotropy of the dielectric constant of the core material ($\epsilon_{\|}\epsilon_{\perp}<0$). The feasibility of the fabrication of such unusual materials will be discussed in Section 3.

B. The Effect of Finite Wall Conductance

In this section we consider the practical realization of the system described above, in which the anisotropic core material is surrounded by metallic walls. The electromagnetic properties of metals at high frequencies are dominated by the dynamics of the free-electron plasmalike gas. Following the approach described in Ref. 38 it is possible to write down the high-frequency effective permittivity of metal in Drude form:

$$\epsilon_m(\omega)=\epsilon_\infty-\frac{\Omega_{\mathrm{pl}}^2}{\omega(\omega+i\tau)}, \tag{7}$$

where the constant term ϵ_∞ describes the contribution of the bound electrons, τ is responsible for EM losses due to (inelastic) processes, and $\Omega_{\mathrm{pl}}=N_e e^2/m_{\mathrm{eff}}$ is the plasma frequency with N_e, e, and m_{eff} being the free-electron concentration, charge, and effective mass, respectively. Note that for $\omega<\Omega_{\mathrm{pl}}/\sqrt{\epsilon_\infty}$ the permittivity of the metal becomes negative $\epsilon_m'<0$ (here and below single and double prime denote the real and imaginary parts, respectively). For most "good" metals (Ag,Al,Au) the plasma frequency is of the order of 10 eV and $\epsilon_\infty\approx 1$, which means that ϵ_m' is negative from optical to gigahertz frequencies. The losses, given by the parameter $\epsilon_m''/|\epsilon_m'|\ll 1$ are typically small in these spectral ranges.

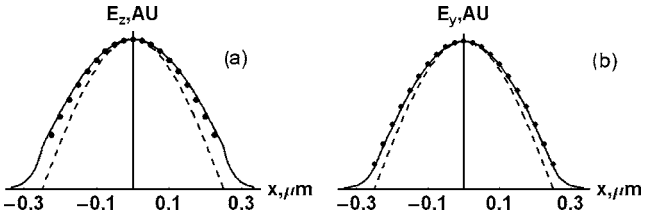

Fig. 2. Cross-section of the field in the planar waveguide with hollow $d=0.5$ μm thick core. Dashed curve, the case of $\epsilon_m=-\infty$ (perfect metal boundary); solid curve, Ag boundaries for $\lambda=0.85$ μm; dots, κ calculated using Eq. (9). (a) TM and (b) TE modes are shown.

Similar to the case of perfectly conducting waveguide walls, the structure of the modes in the system can be derived from the dependence of the longitudinal (z) field component on the x coordinate, which has $\cos(\kappa x)$ or $\sin(\kappa x)$ behavior, depending on its symmetry. The exact value of the mode parameter κ is given by the requirement of the in-plane (y,z) field components' continuity throughout $x=\pm d/2$ planes. For symmetric (cosine) mode profile, we obtain

$$\tan\left[\frac{\kappa^{(\mathrm{TM})}d}{2}\right]=-\frac{\epsilon_m\kappa^{(\mathrm{TM})}}{[k^2\epsilon_{\|}^2(\epsilon_\perp-\epsilon_m)-\kappa^{(\mathrm{TM})^2}\epsilon_{\|}\epsilon_\perp]^{1/2}},$$

$$\tan\left[\frac{\kappa^{(\mathrm{TE})}d}{2}\right]=\frac{[k^2(\epsilon_{\|}-\epsilon_m)-\kappa^{(\mathrm{TE})^2}]^{1/2}}{\kappa^{(\mathrm{TE})}}. \tag{8}$$

In the limit of $\epsilon_m\to-\infty$, these equations yield the values $\kappa_0=\pi(2j+1)/d$, used in Subsection 2.A. As we previously noted, these values correspond to the well-known condition of zero mode magnitude at the waveguide boundary. In the limit of sufficiently large $|\epsilon_m|$ it is possible to find the correction to the above values of the mode parameter κ. Specifically,

$$\kappa^{(\mathrm{TM})}\approx\kappa_0\left(1-\frac{2k\epsilon_{\|}}{\kappa_0^2 d\sqrt{-\epsilon_m}}\right),$$

$$\kappa^{(\mathrm{TE})}\approx\kappa_0\left(1-\frac{2}{kd\sqrt{-\epsilon_m}}\right). \tag{9}$$

As the mode parameter κ plays a role of an inverse confinement length of the mode in x direction, the negative κ correction signifies the "mode expansion" into the waveguide wall region. Such a mode expansion is illustrated in Fig. 2.

The immediate effect of such a change in the mode structure is the change of the effective phase velocity, given by the refraction index

$$n^{(\mathrm{TM})}\approx\pm\sqrt{\epsilon_\perp\nu_0}\left(1+\frac{2}{kd\nu_0\sqrt{-\epsilon_m}}\right),$$

$$n^{(\mathrm{TE})}\approx\sqrt{\epsilon_{\|}\nu_0}\left(1+\frac{2\kappa_0^2}{k^3 d\epsilon_{\|}\nu_0\sqrt{-\epsilon_m}}\right), \tag{10}$$

where $\nu_0=1-\kappa_0^2/(\epsilon_{\|}k^2)$. As was described above, the sign of the refraction index for the TM polarization has to be se-

lected positive for $\epsilon_\perp > 0$; $\nu > 0$, and negative for $\epsilon_\perp < 0$; $\nu < 0$.

Penetration of the mode into the waveguide wall region has another effect on the wave propagation. Namely, the finite value of the ϵ_m'' introduces an additional (with respect to the core material) absorption into the system. As a result, the magnitude of a mode will exponentially decay as it propagates through the system. Such an attenuation can be related to the imaginary part of the effective refractive index through $E \propto \exp(-n''\mathrm{k}z)$. In the limit of small absorption in the metal ($\epsilon_m''/|\epsilon_m'| \ll 1$) the "waveguide-induced" mode decay is described by

$$n^{(\mathrm{TM})''} \approx \frac{1}{kd}\left(\frac{\epsilon_\perp}{\nu_0|\epsilon_m|}\right)^{1/2}\frac{\epsilon_m''}{|\epsilon_m'|},$$

$$n^{(\mathrm{TE})''} \approx \frac{\kappa_0^2}{k^3 d(\epsilon_\parallel \nu_0|\epsilon_m|)^{1/2}}\frac{\epsilon_m''}{|\epsilon_m'|}. \tag{11}$$

Note that in agreement with causality principle[7,25] the losses in the system are positive, regardless of the sign of the refractive index.

Using Eq. (11) we estimate that for wavelengths $\lambda \geqslant 850$ nm, the losses introduced by silver waveguide walls are substantially small ($n''/n \lesssim 0.01$).

3. ANISOTROPIC NANOPLASMONIC COMPOSITES

We now consider the fabrication perspectives of the material with strong optical anisotropy required for NIM waveguide core region. A number of naturally occurring materials with the required properties exist at terahertz or far-IR frequencies; some examples include Bi and sapphire.[36] Unfortunately, no known material exhibits anisotropy exceeding 30% at optical or IR spectral range. Here we propose to take advantage of a new class of nanoengineered media known as metamaterials.[39] In these composites, nanostructured particles are used as meta atoms to achieve the desired EM properties.

To realize the strong optical anisotropy we propose to use a combination of plasmonic or polar particles (providing the negative permittivity) and dielectric media (having $\epsilon > 0$). If the characteristic size of inhomogeneities and their typical separation are much smaller than the wavelength of incident radiation, the composite structure typically supports plane-wave-like modes. The EM properties of these modes can be described in terms of the effective dielectric constant ϵ_{eff}[25]:

$$\langle D(r)\rangle_\alpha = \langle \epsilon(r)_{\alpha,\beta} E(r)_\beta\rangle = \epsilon_{\mathrm{eff}_{\alpha,\beta}}\langle E(r)\rangle_\beta, \tag{12}$$

where the angle brackets denote the averaging over the microscopically large (multiparticle), macroscopically small (subwavelength) spatial area; Greek indices denote Cartesian components; and summation over repeated indices is assumed. Since the size of a particle a typically enters Maxwell equations in the combination ka,[25] all size-related effects play a minor role in the considered quasi-static averaging process. Therefore we note that the composites proposed below are highly tolerant with respect to size variation. Also, since the effects described here originate from the averaged (effective medium) properties of metamaterials, the desired response does not require any periodicity of the particle arrangement and only the *average concentration* has to be controlled during the fabrication step.

Below we present two metamaterial designs of the strongly anisotropic composite for optical and infrared spectrum ranges.

A. Layered System

We first consider the permittivity of a stack of interlacing plasmonic (Ag,Au,Al) or polar (SiC) ($\epsilon_{\mathrm{pl}} < 0$) and dielectric (Si,GaAs) ($\epsilon_d > 0$) layers. We assume that the layers are aligned in the waveguide (y,z) plane (see Fig. 3).

In general, the wave propagation in the layered materials strongly depends on polarization, the ratio of the typical layer thickness δ to the wavelength λ, and the microgeometry of the system, and may become extremely complicated owing to excitation of coupled-surface plasmon-polariton modes, or one-dimensional photonic-crystal-related effects (see, e.g., Refs. 4, 34, and 40–42 and references therein for more comprehensive analysis of the wave dynamics and underlying mode structure in the layered composites). In the considered here case of thin layers ($\delta \ll \{\lambda, d\}$), some of the propagating in the system modes have a plane-wave-like structure and can be successfully described by effective medium approximation. As noted above, the absolute thickness of the layers is not important for the propagation of these modes, and only the average concentration of plasmonic layers N_{pl} plays the role.

To compute ϵ_{eff} we note that the E_y, E_z, and ϵE_x must be continuous throughout the system,[4,25,41,42] leading to

$$\epsilon_\parallel = \epsilon_{\mathrm{eff}_{y,z}} = N_{\mathrm{pl}}\epsilon_{\mathrm{pl}} + (1 - N_{\mathrm{pl}})\epsilon_d,$$

$$\epsilon_\perp = \epsilon_{\mathrm{eff}_x} = \frac{\epsilon_{\mathrm{pl}}\epsilon_d}{(1 - N_{\mathrm{pl}})\epsilon_{\mathrm{pl}} + N_{\mathrm{pl}}\epsilon_d}. \tag{13}$$

The same equations can be obtained as a "quasistatic" limit ($|k_{\{x,y,z\}}\delta| \ll 1$) of 1D photonic crystal formed by periodic layered system.[42]

The effective permittivities for several layered composites are shown in Fig. 4. We note that although the strong anisotropy $\epsilon_\parallel \cdot \epsilon_\perp < 0$ can be easily achieved in the layered system, the actual realizations of the materials with $\epsilon_\parallel > 0, \epsilon_\perp < 0$ required for the high-frequency NIM described here typically have substantial absorption[43] and therefore have a limited range of applications.[10,32]

On the contrary, the materials with $\epsilon_\parallel < 0, \epsilon_\perp > 0$ (achieved, for example by a repeated deposition of Ag-Si layers) form low-loss media. While this configuration has

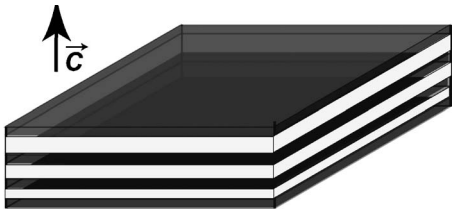

Fig. 3. Schematics of the layered structure described in the text.

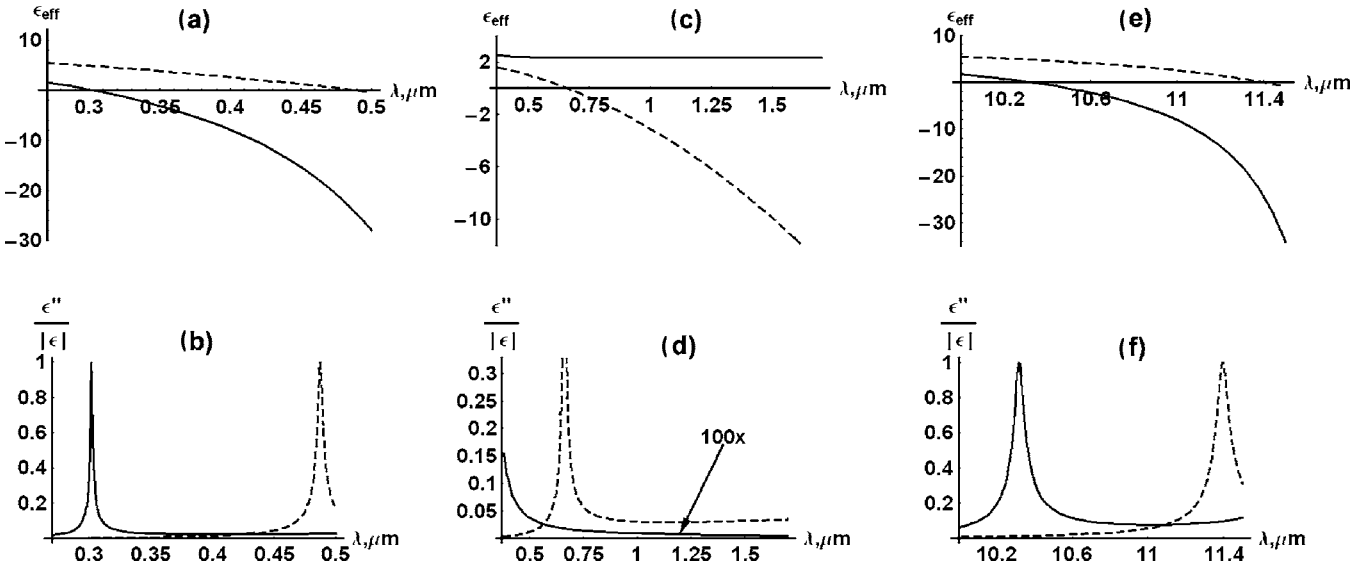

Fig. 4. (a), (c), (e) Real part and (b), (d), (f) absorption of effective $\epsilon_\perp$ (solid curve) and $\epsilon_\parallel$ (dashed curves) for layered systems. (a) and (b) Ag-Si stack, $N_{\mathrm{pl}}=0.6$; (c) and (d) Ag-SiO_2 stack, $N_{\mathrm{pl}}=0.1$ (note the extremely small absorption of this system); (e) and (f) SiC–Si stack, $N_{\mathrm{pl}}=0.1$.

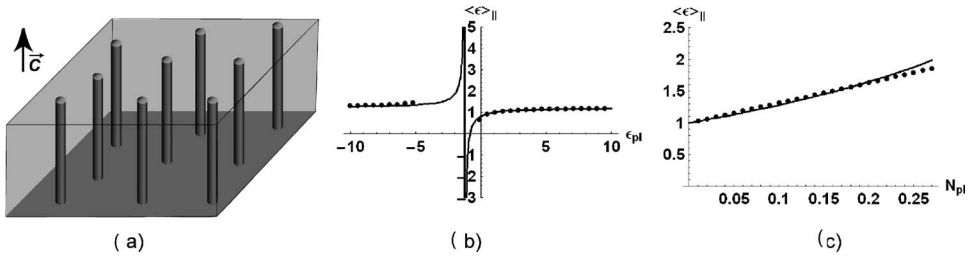

Fig. 5. (a) Schematics of the wired structure described in the text. (b)–(c) comparison of $\langle\epsilon\rangle_\parallel$, calculated using Eq. (14) (solid curve) and derived from numerical solution of Maxwell equations, as described in the text (dots); dependence of $\langle\epsilon\rangle_\parallel$ on dielectric constant of the inclusions for N_{pl} (b) and on concentration for $\epsilon_{\mathrm{pl}}=-10$ (c) is shown.

a positive refraction index, it may be potentially used to concentrate propagating modes in subwavelength areas.[7,42]

B. Aligned Wire Structure

The array of aligned $\epsilon_{\mathrm{pl}}<0$ nanowires embedded in the dielectric ($\epsilon_d>0$) host, schematically shown in Fig. 5, is in some sense a counterpart of the layered system described above. In fact, the boundary conditions now require the continuity of the E_x field, along with the solution of quasistatic equations in the y-z plane. Although in the general case the analytical solution of this problem is complicated, the case of small plasmonic material concentration for nearly normal incidence ($\kappa\approx 0$) is adequately described by the Maxwell–Garnett approximation[25,44–49]:

$$\epsilon_\parallel=\epsilon_{\mathrm{eff}_{y,z}}=\frac{N_{\mathrm{pl}}\epsilon_{\mathrm{pl}}E_{\mathrm{in}}+(1-N_{\mathrm{pl}})\epsilon_d E_0}{N_{\mathrm{pl}}E_{\mathrm{in}}+(1-N_{\mathrm{pl}})E_0},$$

$$\epsilon_\perp=\epsilon_{\mathrm{eff}_x}=N_{\mathrm{pl}}\epsilon_{\mathrm{pl}}+(1-N_{\mathrm{pl}})\epsilon_d, \tag{14}$$

where $E_{\mathrm{in}}=(2\epsilon_d/\epsilon_d+\epsilon_{\mathrm{pl}})E_0$ is the field inside the plasmonic inclusion and E_0 is the excitation field.[50]

To illustrate the validity of the Maxwell–Garnett approximation, we numerically solve the Maxwell equations in the planar geometry using the coupled-dipole approach, described in detail in Refs. 30, 46, and 51. In these calculations the composite is represented by a large number of interacting point dipoles, and the resulting dipole-moment distribution is related to the effective dielectric constant. Figure 5 shows the excellent agreement between the numerical simulations and the analytical result [Eq. (14)].

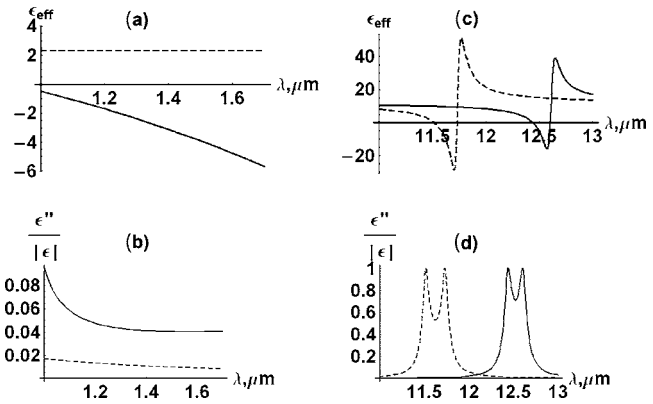

Fig. 6. (a) and (c) Real part and (b) and (d) absorption of effective $\epsilon_\perp$ (solid curves) and $\epsilon_\parallel$ (dashed curves) for wired systems. (a) and (b) Ag-SiO_2 structure (note the relatively small absorption for the NIM regime), $N_{\mathrm{pl}}=0.05$; (c) and (d) SiC-Si structure, $N_{\mathrm{pl}}=0.1$.

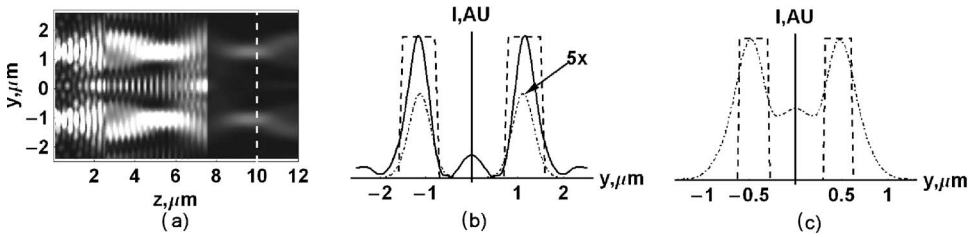

Fig. 7. Imaging by a planar NIM-based lens. $n>0$ region: Si-filled planar waveguide, $d=0.3$ μm; NIM region: planar waveguide with core material described in Fig. 6(a) and 6(b). (a) The intensity distribution in the system with absorption losses is neglected; the LHM region is between $z=2.5$ μm and $z=7.5$ μm. The focal plane corresponds to $z=10$ μm (white dashed line); the slit size is $w=0.75$ μm. (b) Dashed line, emitted radiation; solid line, focal-plane intensity distribution in system described in (a); dash-dotted line, same as solid line, but in the case of real (absorbing) NIM. (c) same as (b), but $w=0.3$ μm (corresponding to far-field resolution limit of the system).

The effective dielectric constants for some composite materials are presented in Fig. 6. Note that in contrast to the layered system described above, these wired composites have extremely low absorption in the near-IR–NIM regime, in a way solving the major problem with the "conventional" design of optical LHMs.

4. IMAGING PROPERTIES OF NONMAGNETIC OPTICAL NIMS

The spatial resolution of any monochromatic optical system can be related to its ability to restore the broad wavevector (k_y) spectrum emitted by a source.[10] In general, the components of this spectrum can be separated into two fundamentally different parts. The waves with $|k_y|<|\omega n|/c$ will propagate away from the source; the relative phase difference between these waves will increase as the distance between the source and the point of observation is increased. In principle, the information about the "thick" ($\gtrsim\lambda/|2n|$) features of the source, contained in these waves, can be accessed at an arbitrary point in space by compensating for this phase difference.

The information about the "fine structure" of the source (features $\lesssim\lambda/|2n|$), however, is contained in the part of the spectrum with $|k_y|\geqslant|\omega n|/c$. The corresponding waves, known as evanescent waves, exponentially decay away from the source. These exponentially decaying waves (along with information they contain) can be directly accessed only in the near-field proximity to the source. Alternatively, some part of the evanescent spectrum can in principle be restored by NIMs via resonant excitation of surface waves[3,10,15–17]; such restoration, however, is strongly suppressed by the material absorption.[10]

Note, that the boundary between the propagating and evanescent parts of the spectrum is defined by both wavelength λ and index of refraction n of a material around the source. Therefore it is possible to achieve the subwavelength far-field resolution using the materials with relatively large values of refraction index.[24]

To illustrate the imaging performance of the proposed system we calculate the propagation of a wave packet formed by a double-slit source through the 5 μm long planar layer of 5% Ag, 95% SiO_2 wire-based NIM core described above [see Fig. 6(a) and 6(b)], embedded in the Si waveguide. We select the thickness of the dielectric core to be $d=0.3$ μm and assume the excitation by the telecom wavelength $\lambda=1.5$ μm. Equations (10) and (14) yield the following values of the refraction index: $n^{(+)}\approx 2.6$, $n^{(\mathrm{NIM})}\approx -2.6+0.05i$.

To calculate the resulting field distribution we first represent the wave packet at the $z=0$ plane as a linear combination of the waveguide modes.[7,36] We then use the boundary conditions at the front and back interfaces of the NIM region to calculate the reflection and transmission of individual mode. The solutions of Maxwell equations are then represented as a sum of solutions for the individual modes.

To better illustrate the imaging properties of the system and distinguish between the effects of negative refractive index and material absorption, we first neglect losses in the NIM core. The resulting intensity distribution in the system is shown in Fig. 7(a). The image formation in the focal plane ($z=10$ μm) of the far-field planar NIM lens can be clearly seen. In Fig. 7(b) we compare the imaging through the planar NIM lens with and without the material absorption and demonstrate that the presence of weak loss does not destroy the far-field imaging, although it reduces the magnitude of the signal.

The resolution Δ of the nonmagnetic NIM structure presented here is limited by the internal wavelength: $\Delta\approx\lambda_{\mathrm{in}}/2=\lambda/|2n|\approx 0.3$ μm [see Fig. 7(c)], similar to the resolution of any far-field imaging system.[10,25,32]

5. CONCLUSIONS

We presented a nonmagnetic nonperiodic design of a system with negative index of refraction. We have further proposed several low-loss nanoplasmonic-based realizations of the proposed structure for optical and infrared frequencies. We have presented analytical description of the effective dielectric permittivity of strongly anisotropic nanostructured composites and showed excellent agreement of the developed theory with results of the numerical solution of Maxwell equations. Finally, we have demonstrated the low-loss, far-field planar NIM lens for $\lambda=1.5$ μm with resolution $\Delta\approx 0.3$ μm.

ACKNOWLEDGEMENTS

The authors thank E. E. Mishchenko and A. L. Efros for fruitful discussions. The research was partially supported by National Science Federation grants DMR-0134736 and ECS-0400615 and by Oregon State University.

V. Podolskiy can be reached via e-mail at viktor.podolskiy@physics.oregonstate.edu.

REFERENCES AND NOTES

1. V. G. Veselago, "The electrodynamics of substances with simultaneously negative values of ϵ and μ," Sov. Phys. Usp. **10**, 509–514 (1968).
2. J. B. Pendry and D. R. Smith, "Reversing light with negative refraction," Phys. Today **57**(6), 37–43 (2004).
3. J. B. Pendry, "Negative refraction makes a perfect lens," Phys. Rev. Lett. **85**, 3966–3969 (2000).
4. G. Shvets, "Photonic approach to making a materials with a negative index of refraction," Phys. Rev. B **67**, 035109-1–8 (2003).
5. A. L. Pokrovsky and A. L. Efros, "Lens based upon the use of left-handed materials," Appl. Opt. **42**, 5701–5705 (2003).
6. V. M. Agranovich, Y. R. Shen, R. H. Baughman, and A. A. Zakhidov, "Linear and nonlinear wave propagation in negative refraction metamaterials," Phys. Rev. B **69**, 165112-1–7 (2004).
7. V. A. Podolskiy and E. E. Narimanov, "Strongly anisotropic waveguide as a nonmagnetic left-handed system," Phys. Rev. B **71**, 201101(R)-1–4 (2005).
8. I. V. Shadrivov, A. A. Sukhorukov, Y. S. Kivshar, A. A. Zharov, A. D. Boardman, and P. Egan, "Nonlinear surface waves in left-handed materials," Phys. Rev. E **69**, 016617-1–9 (2004).
9. N. Fang, H. Lee, C. Sun, and X. Zhang, "Sub-diffraction limited optical imaging with a silver superlens," Science **308**, 534–537 (2005).
10. V. A. Podolskiy and E. E. Narimanov, "Near-sighted superlens," Opt. Lett. **30**, 75–77 (2005).
11. D. R. Smith, D. Schurig, M. Rosenbluth, S. Schultz, S. A. Ramakrishna, and J. B. Pendry, "Limitations of subdiffraction imaging with a negative refractive index slab," Appl. Phys. Lett. **82**, 1506–1508 (2003).
12. R. Merlin, "Analytical solution to the almost-perfect-lens problem," Appl. Phys. Lett. **84**, 1290–1292 (2004).
13. K. J. Webb, M. Yang, D. W. Ward, and K. A. Nelson, "Metrics for negative refractive index materials," Phys. Rev. E **70**, 035602(R)-1 4 (2004).
14. I. I. Smolyaninov, J. Elliott, A. V. Zayats, and C. C. Davis, "Far-field optical microscopy with a nanometer-scale resolution based on the in-plane image magnification by surface plasmon polaritons," Phys. Rev. Lett. **94**, 057401-1–4 (2005).
15. A. Grbic and G. V. Eleftheriades, "Overcoming the diffraction limit with a planar left-handed transmission-line lens," Phys. Rev. Lett. **92**, 117403-1–4 (2004).
16. G. Shvets and Y. A. Urzhumov, "Engineering the electromagnetic properties of periodic nanostructures using electrostatic resonances," Phys. Rev. Lett. **93**, 243902-1–4 (2004).
17. G. Shvets and Y. A. Urzhumov, "Electric and magnetic properties of subwavelength plasmonic crystals," J. Opt. B **7**, S23–S31 (2005).
18. S. A. Darmanyan, M. Neviere, and A. A. Zakhidov, "Nonlinear surface waves at the interfaces of left-handed electromagnetic media," Phys. Rev. E **72**, 0366151-6 (2005).
19. D. R. Smith, W. J. Padilla, D. C. Vier, S. C. Nemat–Nasser, and S. Shultz, "Composite medium with simultaneously negative permeability and permittivity," Phys. Rev. Lett. **84**, 4184–4187 (2000).
20. C. Parazzoli, R. Greegor, K. Li, B. E. C. Koltenbah, and M. Tanielian, "Experimental verification and simulation of negative index of refraction using Snell's law," Phys. Rev. Lett. **90**, 107401-1–4 (2003).
21. P. V. Parimi, W. T. Lu, P. Vodo, and S. Sridhar, "Imaging by flat lens using negative refraction," Nature **426**, 404–404 (2003).
22. S. Foteinopoulou, E. N. Economou, and C. M. Souloulis, "Refraction in a media with negative refractive index," Phys. Rev. Lett. **90**, 107402-1–4 (2003).
23. Z. Lu, S. Shi, C. A. Schuetz, and D. W. Prather, "Experimental demonstration of negative refraction imaging in both amplitude and phase," Opt. Express **13**, 2007–2012 (2005).
24. I. I. Smolyaninov, J. Elliott, G. Wurtz, A. V. Zayats, and C. C. Davis, "Immersion microscopy based on photonic crystal materials," arXiv: cond-mat/0505351-1–23 (2005).
25. L. D. Landau, E. M. Lifshitz, and L. P. Pitaevskii, *Course of Theoretical Physics*, 2nd ed. (Reed, 1984). Vol. 8.
26. T. Y. Yen, W. J. Padilla, N. Fang, D. C. Vier, D. R. Smith, J. B. Pendry, D. N. Basov, and X. Zhang, "THz magnetic response from artificial materials," Science **303**, 1494–1496 (2004).
27. V. M. Shalaev, W. Cai, U. Chettiar, H.-K. Yuan, A. K. Sarychev, V. P. Drachev, and A. V. Kildishev, "Negative index of refraction in optical metamaterials," arXiv: physics/050491-1–17 (2005).
28. S. O'Brien, D. McPeake, S. A. Ramakrishna, and J. B. Pendry, Phys. Rev. B **69**, 241101 (2004).
29. V. A. Podolskiy, A. K. Sarychev, and V. M. Shalaev, "Plasmon modes in metal nanowires," J. Nonlinear Opt. Phys. Mater. **11**, 65–74 (2002).
30. V. A. Podolskiy, A. K. Sarychev, and V. M. Shalaev, "Plasmon modes and negative refraction in metal nanowire composites," Opt. Express **11**, 735–745 (2003).
31. S. Linden, C. Enkrich, M. Wegener, J. Zhou, T. Koschny, and C. M. Soukoulis, "Magnetic response of metamaterials at 100 terahertz," Science **306**, 1351–1353 (2004).
32. It can be shown[10,33] that for losses $\{\epsilon,\mu\}''/|\{\epsilon,\mu\}'|>0.3$ even the near-field resolution of the NIM-based system is smaller than that of conventional near-field optics.
33. V. A. Podolskiy, N. A. Kuhta, and G. Milton, "Optimizing the superlens: manipulating geometry to enhance the resolution," Appl. Phys. Lett. **87**, 231113 1–3 (2005).
34. M. Notomi, "Theory of light propagation in strongly modulated photonic crystals: refractionlike behavior in the vicinity of the photonic band gap," Phys. Rev. B **62**, 10696–10705 (2000).
35. A. L. Efros and A. L. Pokrovsky, "Dielectric photonic crystals as medium with negative electric permittivity and magnetic permeability," Solid State Commun. **129**, 643–647 (2004).
36. V. A. Podolskiy, L. Alekseev, and E. E. Narimanov, "Strongly anisotropic media: the THz perspectives of left-handed materials," J. Mod. Opt. **52**, 2343–2349 (2005).
37. The TEM wave formally corresponds to a TM wave with $\kappa=0$. As seen from Eqs. (1)–(3), such a wave cannot propagate in NIM described here.
38. E. M. Lifshitz and L. P. Pitaevskii, *Course of Theoretical Physics* (Reed, 1984), Vol. 10.
39. See, e.g., J. Opt. A, Special Issue on Nanostructured Optical Meta-Materials **7**, (2005).
40. L. M. Brekhovskikh, *Waves in Layered Media*, 2nd ed. (Academic, 1980).
41. A. Alú and N. Engheta, "An overview of salient properties of planar guided-wave structures with double-negative (DNG) and single-negative (SNG) layers," in *Negative Refraction Metamaterials: Fundamental Properties and Applications*, G. V. Eleftheriades and K. G. Balmain, eds. (Wiley, 2005).
42. A. A. Govyadinov and V. A. Podolskiy, "Using photonic crystals to build optical funnels," Phys. Rev. Lett., submitted for publication.
43. This particular realization of layered NIM structure for IR frequencies was earlier proposed in Ref. 4.
44. O. Levy and D. Stroud, "Maxwell–Garnett theory for mixtures of anisotropic inclusions: application to conducting polymers," Phys. Rev. B **56**, 8035–8046 (1997).
45. A. Lakhtakia, B. Michel, and W. S. Weiglhofer, "The role of anisotropy in the Maxwell–Garnett and Bruggeman formalisms for uniaxial particulate composite media," J. Phys. D **30**, 230–240 (1997).
46. V. A. Podolskiy and E. E. Narimanov, "Nanoplasmonic approach to strongly anisotropic optical materials," in *Conference on Lasers and Electro-optics/Quantum Electronics Conference/Photonics Applications Systems Technologies*, OSA Trends in Optics and Photonics Series Optical Society of America (2005), paper JThC3.
47. J. B. Pendry, A. J. Holden, W. J. Stewart, and I. Youngs, "Extremely low frequency plasmons in metallic

mesostructures," Phys. Rev. Lett. **76**, 4773–4776 (1996).
48. G. Shvets, A. K. Sarychev, and V. M. Shalaev, "Electromagnetic properties of three-dimensional wire arrays: photons, plasmons, and equivalent circuits," Proc. SPIE **5218**, 156–165 (2003).
49. A. L. Pokrovsky and A. L. Efros, "Nonlocal electrodynamics of two dimensional wire mesh photonic crystals," Phys. Rev. B **65**, 04510-1–8 (2002).
50. Similar to any nanostructured composite material, the dielectric constant of nanocylinder array may be influenced by the spatial dispersion.[25,38,48,49] We defer the detailed study of these effects to our later work.
51. V. A. Podolskiy, A. K. Sarychev, E. E. Narimanov, and V. M. Shalaev, "Resonant light interaction with plasmonic nanowire systems," J. Opt. A, Pure Appl. Opt. **7**, S32–S37 (2005).